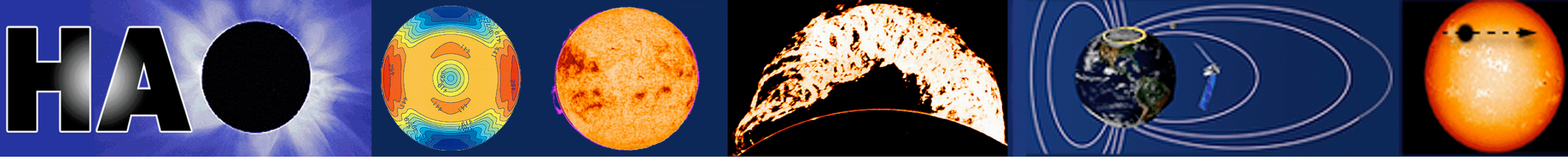

M1 (and E1) Coronal Lines and Magnetic Fields

Philip Judge

1. What do we want to know?
2. What can we actually measure?
3. What kind of strategies can we use to bridge the gap?
4. What might we expect from DKIST?

What do we want to know?

- *what are the root causes of*
  - *coronal heating*
  - *coronal dynamics*
  - *Flaring...*

magnetic free energy (total - potential)

Lorentz force **j**×**B** ~ **curl B** × **B**

requires measurements of **B**(**r**,t) on small length and time scales, e.g.

$50\ \mathrm{Mm}/0.1c_A \sim 250\ \mathrm{sec}$

- *the magnetic solar cycle*

B, magnetic helicity ∫ **A.B** dV over a solar cycle (w/ gauge)

requires measurements of **B**(**r**,t) on global length and time scales

What we can measure?

- **S** = (I,Q,U,V) on the 2D plane of sky as function of λ
- Actually, $\{I+S_i, I-S_i\}$, $i=1...3$, $I=S_0$, sequentially

- BUT we want 3D vector magnetic field from 2D data
  - Impossible
  - Further information required
    - » Knowledge of geometry, 1-point quadratures, *atomic alignment* σ
    - » E.g. tomography (solar rotation and/or spacecraft)
    - » Models from surface and heliospheric boundary conditions

DEM ξ(T)dT from UV/EUV/X-ray

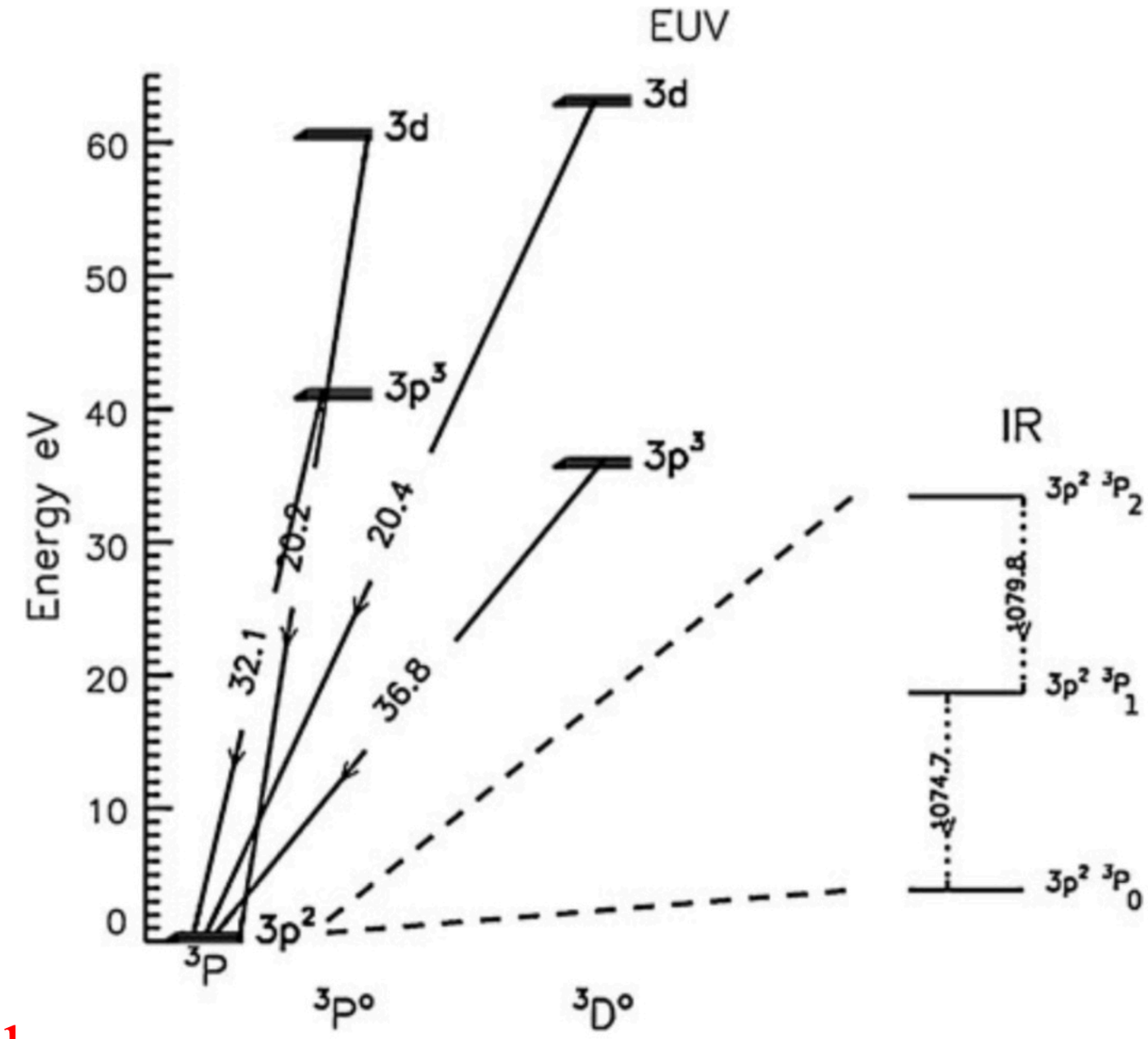

Figure 2 Term diagram for Fe XIII showing the strongest E1 transitions of each multiplet, and the M1 lines among the levels of the ground term. The 1074.7 nm line has upper-level $J = 1$, lower $J = 0$. Each configuration shown has EUV line ratios sensitive to density and photospheric radiation field as a result of the competition for sub-level populations in the ground term.

E1 A ~10^{10} /sec. EUV

M1 A ~ E1 $\alpha^2 \lambda^{-3}$

3 / sec IR

M1 lines in strong field

Limit of Hanle effect

Something familiar
DEM ξ(T)dT

$$I_0(\hat{\mathbf{k}}) = \int_0^\infty I_0(\nu, \hat{\mathbf{k}})\, d\nu = \frac{h\nu_0}{4\pi} \int_{\Delta s} N_J\, A_{J\to J_0}\, ds \qquad \text{erg cm}^{-2}\ \text{sr}^{-1}\ \text{s}^{-1}$$

$$N_{J_0} n_e C_{J_0\to J} = N_J (A_{J\to J_0} + n_e C_{J\to J_0}) \approx N_J A_{J\to J_0},$$

$$N_J A_{J\to J_0} = N_{J_0} n_e C_{J_0\to J} = \frac{N_{J_0}}{N_{ion}} \frac{N_{el}}{N_H} \frac{N_H}{n_e} \left[\frac{N_{ion}}{N_{el}} C_{J_0\to J}\right] n_e^2,$$

$$= const.\ A_{el}\ 0.8\ g(T_e)\ n_e^2,$$

$$I_0(\hat{\mathbf{k}}) = \frac{h\nu_0}{4\pi} \int_{\Delta s} const.\, A_{el}\, 0.8\, g(T_e)\, n_e^2\, ds,$$

$$= \int_{\Delta T_e} G(T_e)\xi(T_e) dT_e,$$

Atomic properties

Plasma properties

Something familiar
DEM ξ(T)dT

The meaning of ξ(T)dT

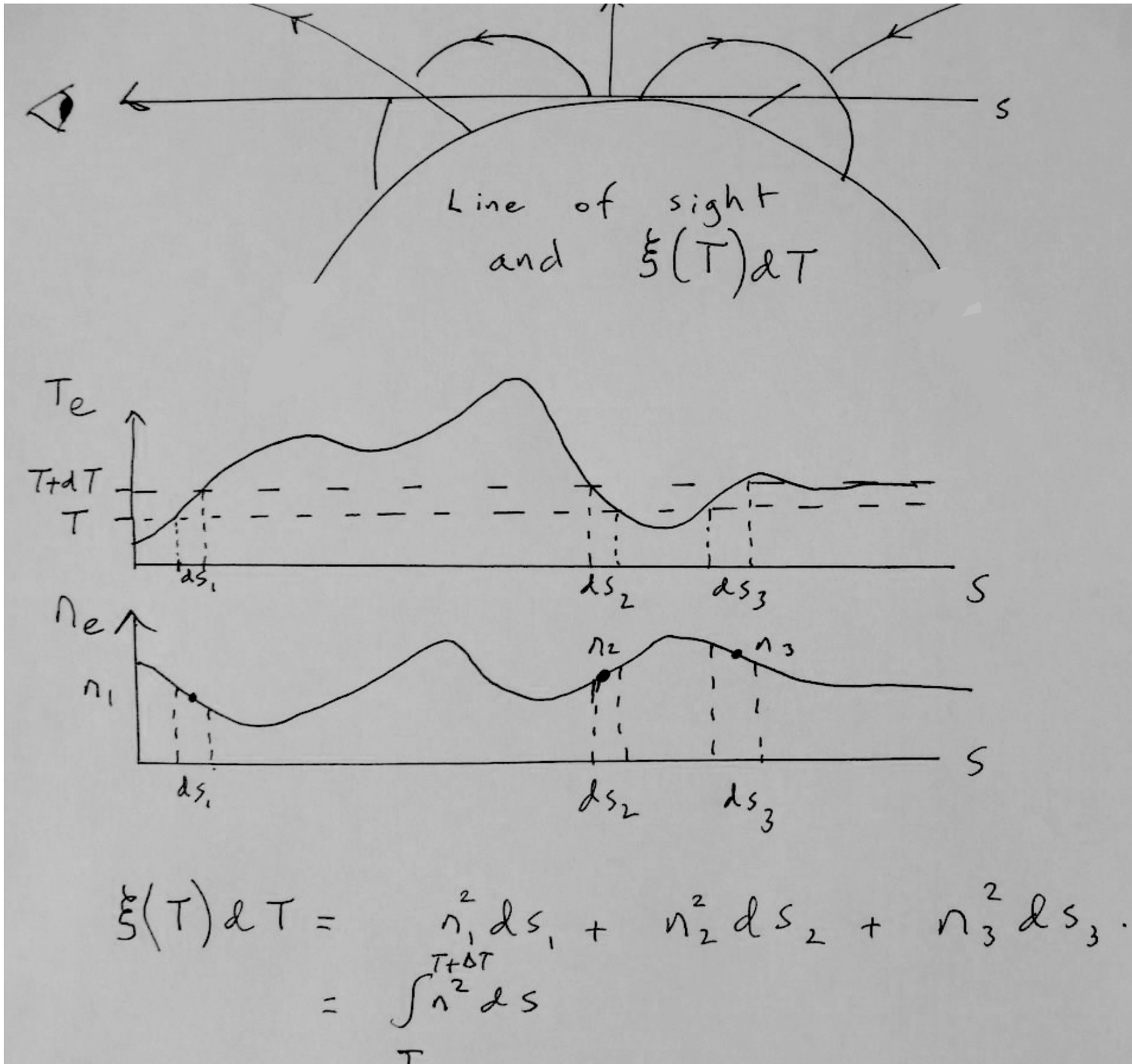

$$\xi(T)\,dT = n_1^2\,ds_1 + n_2^2\,ds_2 + n_3^2\,ds_3 \cdots$$

$$= \int_T^{T+\Delta T} n^2\,ds$$

Polarization of spectral lines

- Classical: selection of different oscillators
- Quantum: selection of M in |α JM>
- Two origins

1. External fields separates energies of M, M' **Zeeman effect**
2. Anisotropy and polarized incident radiation **Atomic poln**

- Interplay between 1. and 2. gives the **Hanle effect** (not Dis cussed here, all M1 lines are Hanle-saturated)

Photospheric vs coronal Line profiles

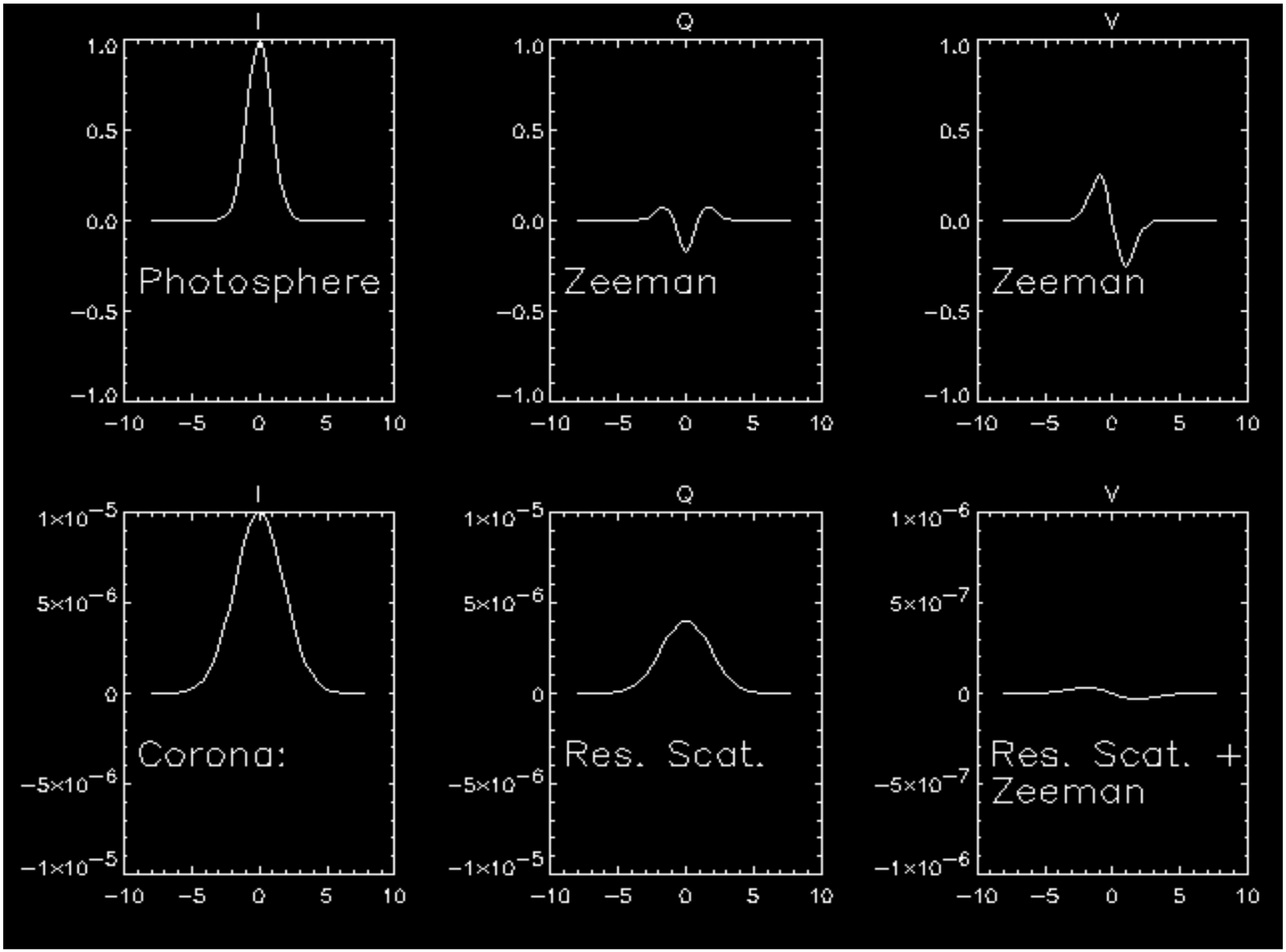

IQUV Standard **Zeeman effect**

Q from **anisotropy σ**
V from **Zeeman effect**

Photospheric vs coronal Line profiles

- Naively:
  - photosphere " λ maps into τ_λ (z)" (Eddington-Barbier relation): OK
  - in the corona ~~λ maps into τ_λ (z)~~, as I_i forms along line of sight *s* in direction ***k***

$$I_i(\nu, \hat{\boldsymbol{k}}) = \int_{\Delta s} \varepsilon_i(\nu, \hat{\boldsymbol{k}})\, ds \text{ ergs cm}^{-2} \text{ sr}^{-1} \text{ s}^{-1} \text{ Hz}^{-1}$$

- So we must focus on $\varepsilon_i(\nu)$

- First look at some simulated/real data

Example: plane of sky source, linear polarization

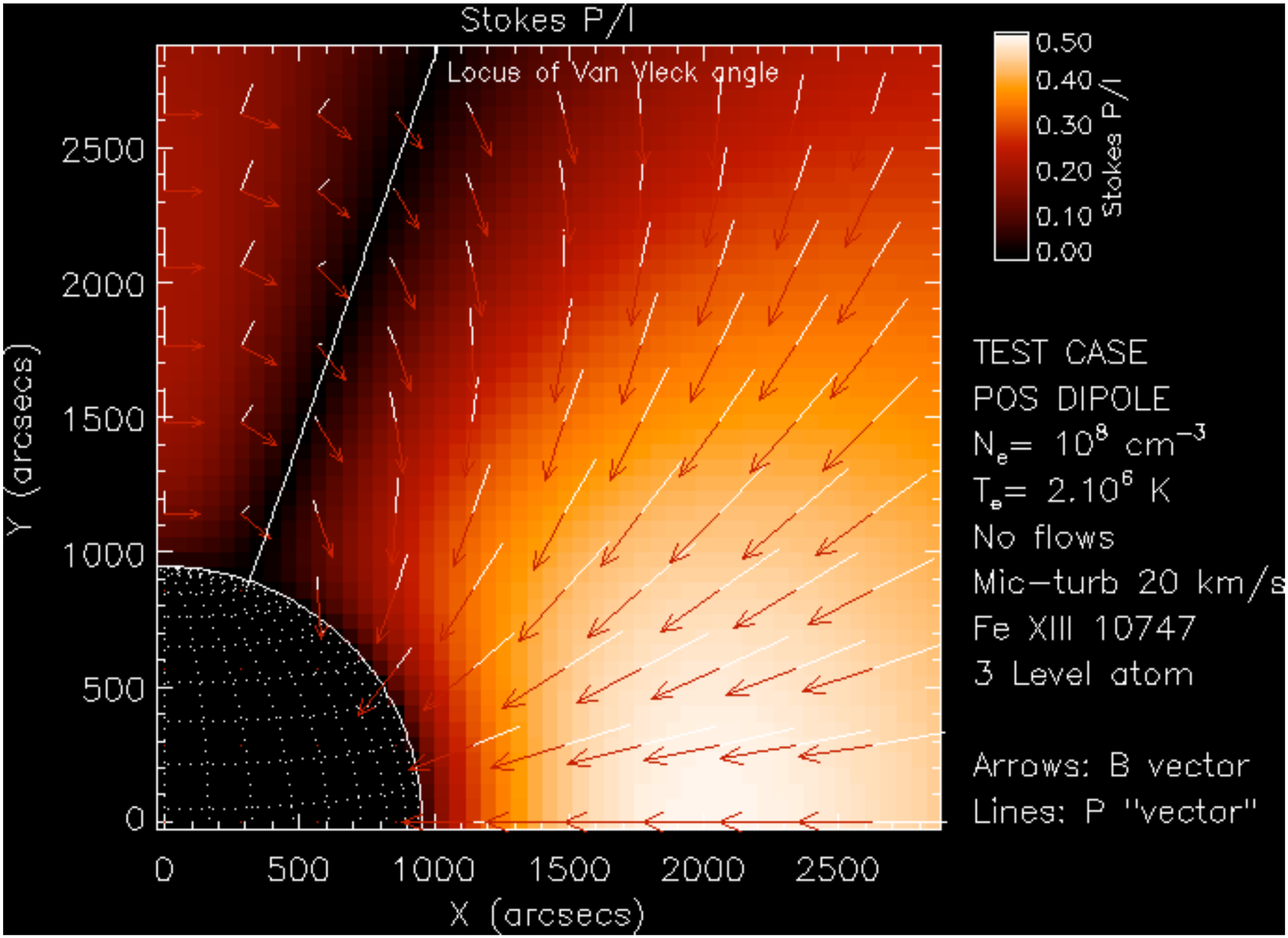

Example: KELP (NSO/HAO) 1970s/1980s

- Linear polarization,
  Fe XIII 1.0747
- D=40cm, f/16 coronagraph
- 2 diodes per beam, 2 beams
  - on-band (0.56nm) off- (2.2 nm)
- IQU only (V=0)
- 100Hz modulation
- 1 arcmin aperture, 5s integ.
- map~ hours
- P/I ~ 0.01
- useful data nearly everywhere

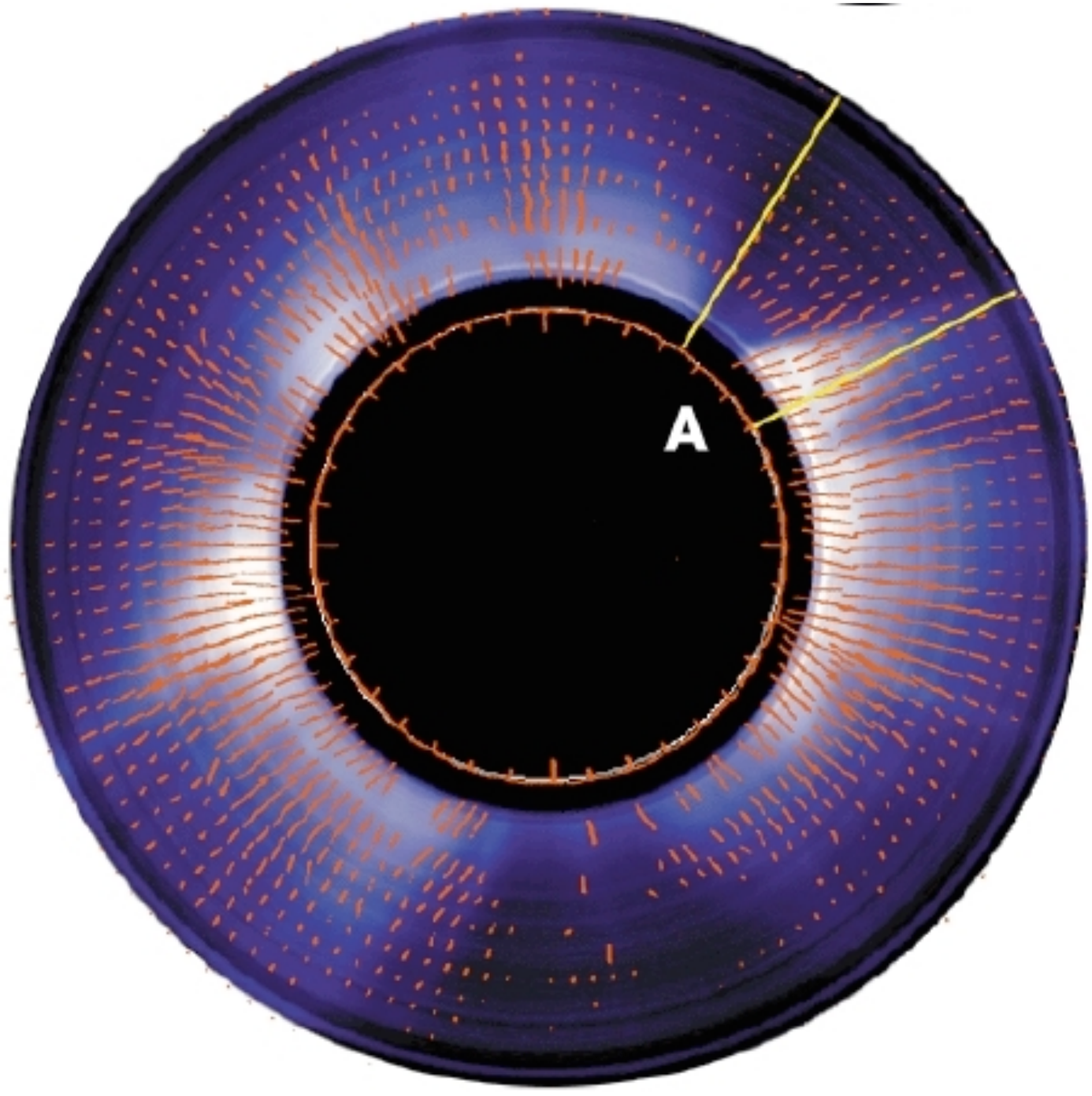

Nuts and bolts $\varepsilon_i(\nu)$: geometry

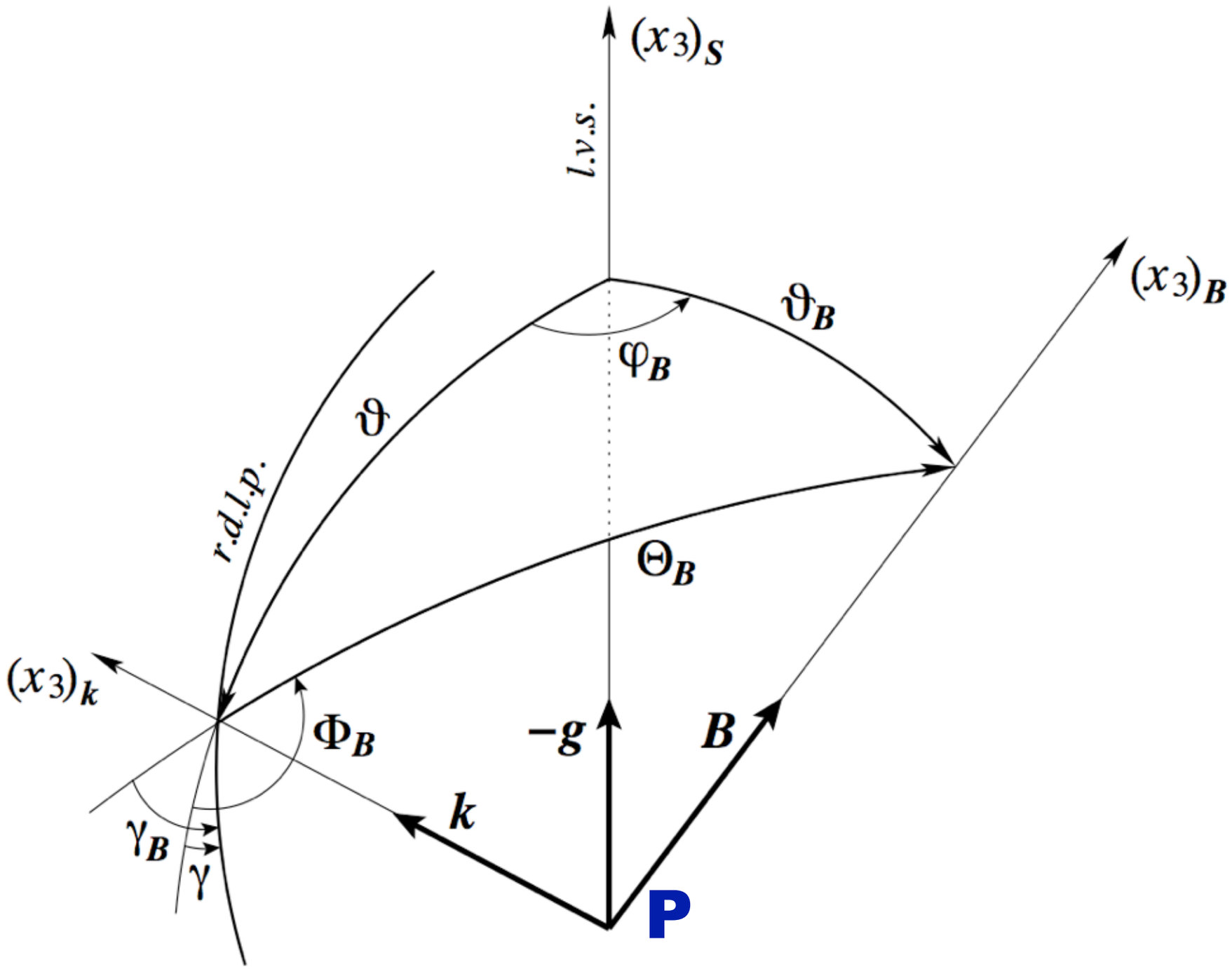

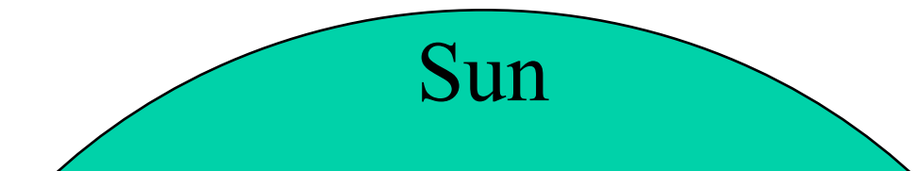

Nuts and bolts: $\varepsilon_i(\nu)$

$$\varepsilon_0^{(0)}(\nu,\hat{\mathbf{k}}) = \epsilon_{JJ_0}\,\phi(\nu_0-\nu)\left[1+D_{JJ_0}\,\sigma_0^2(\alpha_0 J)\,\mathcal{T}_0^2(0,\hat{\mathbf{k}})\right]\ ,$$

$$\varepsilon_i^{(0)}(\nu,\hat{\mathbf{k}}) = \epsilon_{JJ_0}\,\phi(\nu_0-\nu)\,D_{JJ_0}\,\sigma_0^2(\alpha_0 J)\,\mathcal{T}_0^2(i,\hat{\mathbf{k}})\ , \qquad (i=1,2)$$

$$\varepsilon_3^{(1)}(\nu,\hat{\mathbf{k}}) = -\sqrt{\tfrac{2}{3}}\,\nu_{\rm L}\,\epsilon_{JJ_0}\,\phi'(\nu_0-\nu)\left[\bar{g}_{\alpha_0 J,\alpha_0 J_0}+E_{JJ_0}\,\sigma_0^2(\alpha_0 J)\right]\mathcal{T}_0^1(3,\hat{\mathbf{k}})$$

Nuts and bolts: $\varepsilon_i(\nu)$

$$\varepsilon_0^{(0)}(\nu,\hat{\mathbf{k}}) = \epsilon_{JJ_0}\,\phi(\nu_0-\nu)\left[1+D_{JJ_0}\,\sigma_0^2(\alpha_0 J)\,\mathcal{T}_0^2(0,\hat{\mathbf{k}})\right] ,$$

$$\varepsilon_i^{(0)}(\nu,\hat{\mathbf{k}}) = \epsilon_{JJ_0}\,\phi(\nu_0-\nu)\,D_{JJ_0}\,\sigma_0^2(\alpha_0 J)\,\mathcal{T}_0^2(i,\hat{\mathbf{k}}) , \qquad (i=1,2)$$

$$\varepsilon_3^{(1)}(\nu,\hat{\mathbf{k}}) = -\sqrt{\tfrac{2}{3}}\,\nu_{\mathrm{L}}\,\epsilon_{JJ_0}\,\phi'(\nu_0-\nu)\left[\bar{g}_{\alpha_0 J,\alpha_0 J_0}+E_{JJ_0}\,\sigma_0^2(\alpha_0 J)\right]\mathcal{T}_0^1(3,\hat{\mathbf{k}})$$

- Focus on the role of atomic alignment $\sigma_0{}^2$
- Leading terms in SE equations: $\sigma_0{}^2 \approx k_J(T_e, n_e, \vartheta_{\mathrm{M}})\, v(\vartheta_{\mathrm{B}})$
- $v(\vartheta_{\mathrm{B}}) = 3\cos^2\vartheta_{\mathrm{B}} - 1$ "Van Vleck effect"

Nuts and bolts: $\varepsilon_i(\nu)$

$$\varepsilon_0^{(0)}(\nu,\hat{\mathbf{k}}) = \epsilon_{JJ_0}\,\phi(\nu_0-\nu)\left[1+D_{JJ_0}\,\sigma_0^2(\alpha_0 J)\,\mathcal{T}_0^2(0,\hat{\mathbf{k}})\right] ,$$

$$\varepsilon_i^{(0)}(\nu,\hat{\mathbf{k}}) = \epsilon_{JJ_0}\,\phi(\nu_0-\nu)\,D_{JJ_0}\,\sigma_0^2(\alpha_0 J)\,\mathcal{T}_0^2(i,\hat{\mathbf{k}}) , \qquad (i=1,2)$$

$$\varepsilon_3^{(1)}(\nu,\hat{\mathbf{k}}) = -\sqrt{\tfrac{2}{3}}\,\nu_{\rm L}\,\epsilon_{JJ_0}\,\phi'(\nu_0-\nu)\left[\bar{g}_{\alpha_0 J,\alpha_0 J_0}+E_{JJ_0}\,\sigma_0^2(\alpha_0 J)\right]\mathcal{T}_0^1(3,\hat{\mathbf{k}})$$

- Focus on the role of atomic alignment $\sigma_0{}^2$
- Leading terms in SE equations: $\sigma_0{}^2 \approx k_J(T_e,n_e,\vartheta_{\rm M})\,v(\vartheta_{\rm B})$
- $v(\vartheta_{\rm B}) = 3\cos^2\vartheta_{\rm B}-1$ "Van Vleck effect"

$$\varepsilon_0(\hat{\mathbf{k}}) = \epsilon_{JJ_0}\left[1+k_J(T_e,n_e,\vartheta_{\rm M})\,v(\vartheta_{\rm B})\,\tfrac{1}{2\sqrt{2}}v(\Theta_{\rm B})\right],$$

$$\varepsilon_1(\hat{\mathbf{k}}) = \epsilon_{JJ_0}\,k_J(T_e,n_e,\vartheta_{\rm M})\,v(\vartheta_{\rm B})\;\tfrac{3}{2\sqrt{2}}\cos 2\gamma_{\rm B}\sin^2\Theta_{\rm B},$$

$$\varepsilon_2(\hat{\mathbf{k}}) = \epsilon_{JJ_0}\,k_J(T_e,n_e,\vartheta_{\rm M})\,v(\vartheta_{\rm B})\;\tfrac{-3}{2\sqrt{2}}\sin 2\gamma_{\rm B}\sin^2\Theta_{\rm B},$$

$$\varepsilon_3(\nu,\hat{\mathbf{k}}) = -\epsilon_{JJ_0}\,\nu_{\rm L}\,\phi'(\nu_0-\nu)\;[\bar{g}_{J,J_0}+ak_J(T_e,n_e,\vartheta_{\rm M})\,v(\vartheta_{\rm B})\,]\;\cos\Theta_{\rm B}$$

Nuts and bolts: $\varepsilon_i(\nu)$

- Approximate solutions for σ_0^2 : (within a few %):

  - $k_J(T_e, n_e, \theta_M)$ - statistical eq. equations (θ_M = solar semi-diameter)
    - Positive definite
  - $v(\vartheta_B) = 3\cos^2\vartheta_B - 1$ - geometry of **B**, **g**
    - Changes sign (Van Vleck effect)

  - **Factorization allows some analytical simplifications and further understanding**
  - σ_0^2 is large for low J and for high radiative asymmetry
  - is small for high J and low asymmetry and high collisions
  - Van Vleck can be your friend…

Van Vleck effect

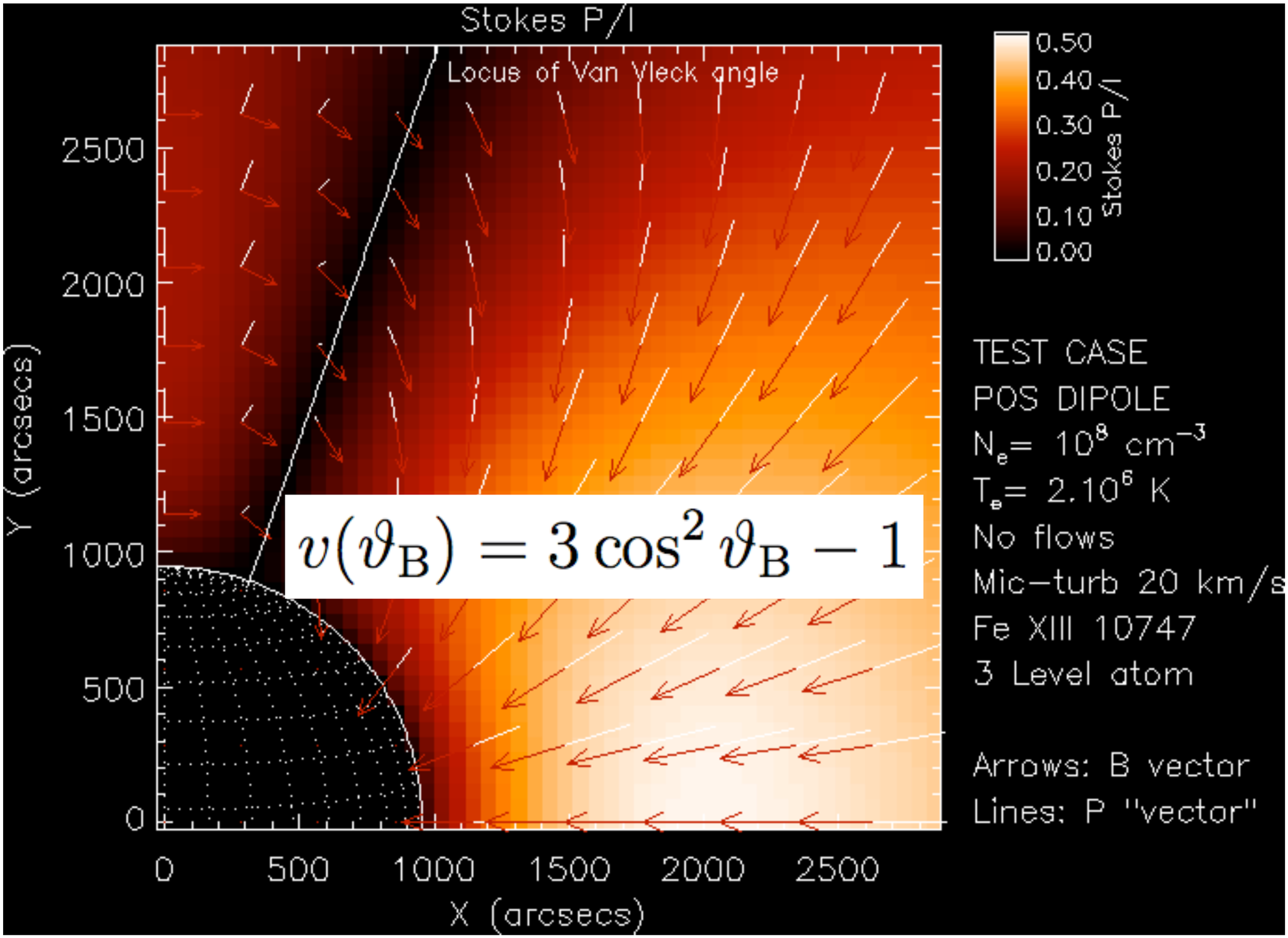

strategies for getting B(x,y,z;t)

- **single point inversions**
  - stand-alone B(LOS) and azimuth*(POS) from $(IQUV)_\lambda$, $dI_\lambda/d\lambda$
  - Alfvén waves: |B| from
    - V_A from V_{phase}(POS) [and much smaller V(LOS) from I_λ]
    - ρ from I_{10798}/I_{10747}, or P/I_{10747} (Querfeld)

- **forward model comparisons**
- **tomography IQUV(x,y,t) -> B(x,y,z)**
  - **Kramar IV(x,y,t) -> B(x,y,z)**

Building blocks: single points in the corona

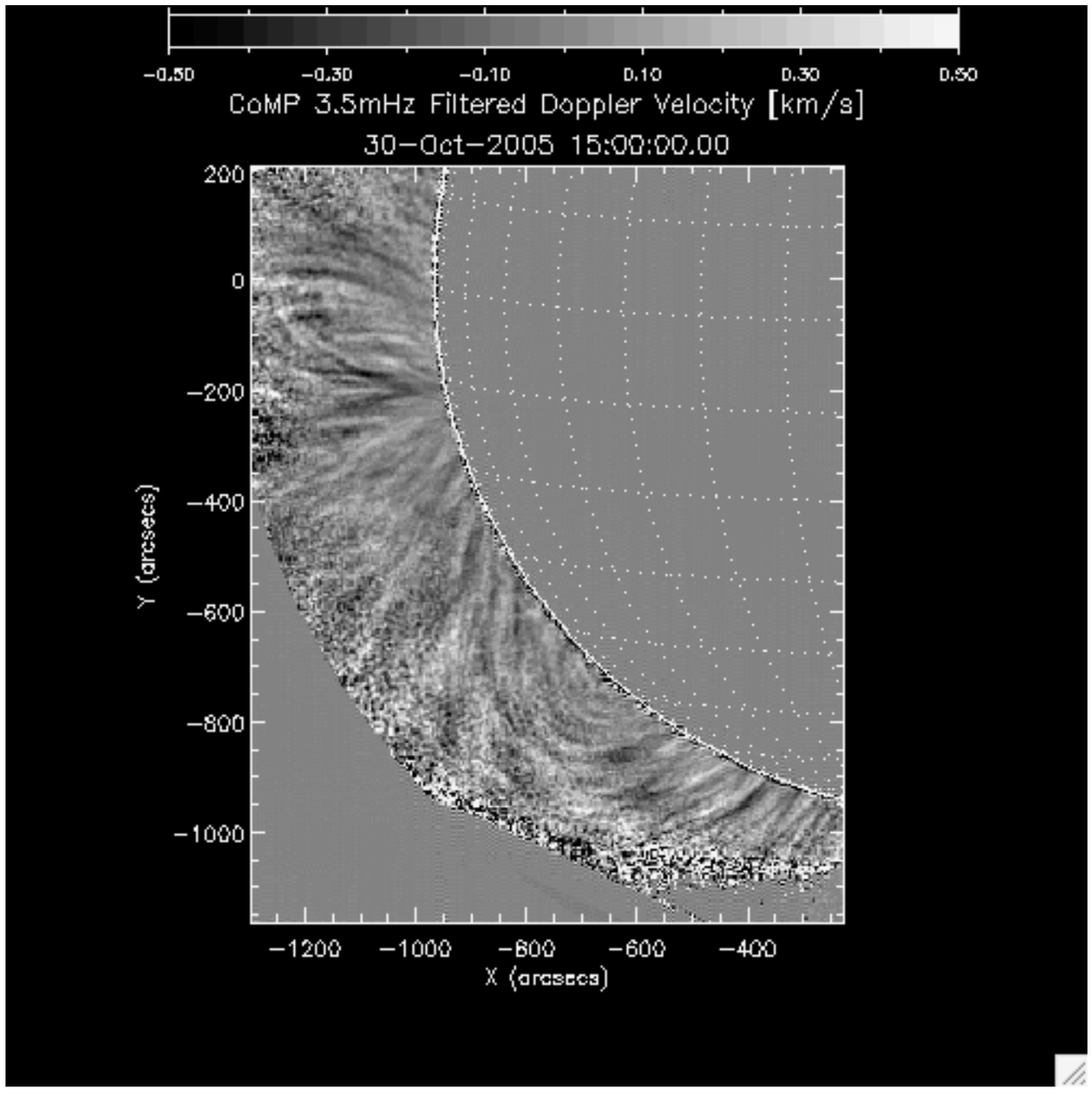

LOS confusion does not remove coherent transverse wave signals

Building blocks: single points in the corona

THE ASTROPHYSICAL JOURNAL, 662:677–690, 2007 June 10

SPECTRAL LINES FOR POLARIZATION MEASUREMENTS OF THE CORONAL MAGNETIC FIELD. V. INFORMATION CONTENT OF MAGNETIC DIPOLE LINES

P. G. JUDGE
High Altitude Observatory, National Center for Atmospheric Research,[1] Boulder, CO 80307-3000
Received 2006 November 28; accepted 2007 February 9

Judge 2007
B(x,y,z=z$_0$): we want (|B|, Θ_B, Φ_B or γ_B)

Table 2. Ambiguities with/without knowledge of atomic alignment $\sigma_0^2(\alpha_0 J)$

Measurements	derived quantities without $\sigma_0^2(\alpha_0 J)$	derived quantities with $\sigma_0^2(\alpha_0 J)$
I, Q, U only	$\gamma_B + n\frac{\pi}{2}$, $\Theta_B \pm n\pi$	$\gamma_B + n\pi$,$\Theta_B \pm n\pi$
I, Q, U, V	$\gamma_B + n\frac{\pi}{2}$, $\Theta_B \pm n\pi$, $\mathbf{B}^* \cdot \hat{\mathbf{k}}$	$\gamma_B + n\pi$, Θ_B, $\lvert\mathbf{B}\rvert$ (see † below)

Note. — n is any integer in the above table, and the magnetic field angles (γ_B, Θ_B) are given between 0 and $\frac{\pi}{2}$. $\mathbf{B}^*$ is the magnetic field evaluated with the magnetograph formula, i.e. ignoring atomic alignment in equation (20). † This case amounts to knowledge of the vector field $\mathbf{B}$ with a POS angle ambiguity of π. This case also applies when the sign of the alignment is known, but the magnitude is ambiguous, but $|\mathbf{B}|$ then has several possible values.

Plowman 2014 solve for B,n, alignment...

HE ASTROPHYSICAL JOURNAL, 792:23 (8pp), 2014 September 1 doi:10.1088/0004-637X/792/1/23

SINGLE-POINT INVERSION OF THE CORONAL MAGNETIC FIELD

JOSEPH PLOWMAN
High Altitude Observatory, National Center for Atmospheric Research, P.O. Box 3000, Boulder, CO 80307-3000, USA; plowman@ucar.edu
Received 2014 May 5; accepted 2014 July 10; published 2014 August 11

ABSTRACT

The Fe XIII 10747 and 10798 Å lines observed in the solar corona are sensitive to the coronal magnetic field in such a way that, in principle, the full vector field at a point on the line of sight can be inferred from their combined polarization signals. This paper presents analytical inversion formulae for the field parameters and analyzes the uncertainty of magnetic field measurements made from such observations, assuming emission dominated by a single region along the line of sight. We consider the case of the current Coronal Multi-channel Polarimeter (CoMP) instrument as well as the future Coronal Solar Magnetism Observatory (COSMO) and Advanced Technology Solar Telescope (ATST) instruments. Uncertainties are estimated with a direct analytic inverse and with a Markov Chain Monte Carlo algorithm. We find that (in effect) two components of the vector field can be recovered with CoMP, and well recovered with COSMO or ATST, but that the third component can only be recovered when the solar magnetic field is strong and optimally oriented.

Key words: methods: data analysis – Sun: corona – Sun: magnetic fields – techniques: polarimetric

Judge 2007

The more you know about the atomic alignment, the nearer to vector B you will get

second strategy: forward models vs data

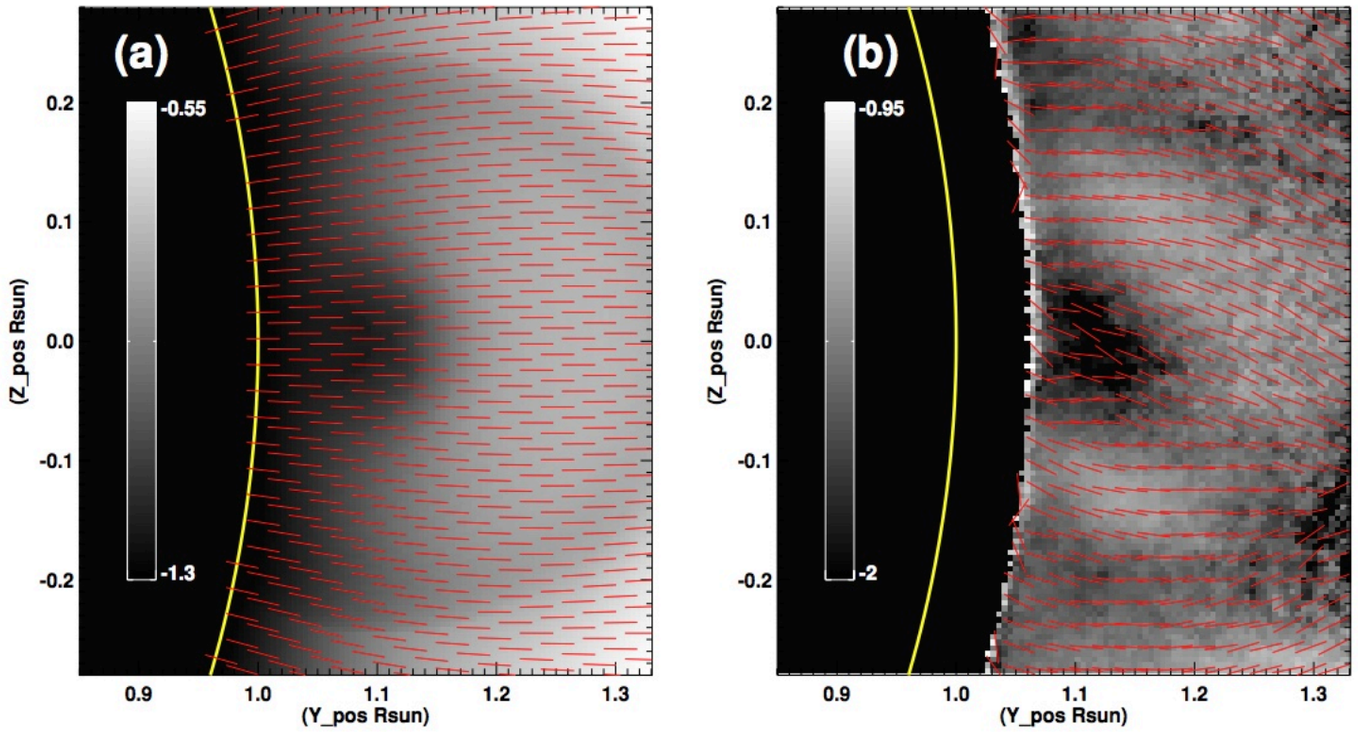

Figure 3. LOS-integrated Stokes P/I for (a) forward-calculated spheromak configuration and (b) CoMP observations of 2005 April 21, southwest cavity.

"There are more things in heaven and earth, Horatio, than are dreamt of in your philosophy." -- Hamlet

third strategy: tomography

Vector tomography

- IV only Kramar, Inhester, Solanki 2006. (nb use of “Hanle”)
- IV or IQU only Kramar & Inhester 2007
  - stationary, rotating corona
  - inversion I,V
  - alignment explicitly zero. With D= “data”,

$$\begin{pmatrix} D_V \\ D_{(Q,U)} \end{pmatrix} = \int_{\mathrm{LOS}} \begin{pmatrix} \epsilon_V \\ \epsilon_{(Q,U)} \end{pmatrix} d\ell \sim \int_{\mathrm{LOS}} \begin{pmatrix} B_{\parallel} \\ \mathbf{B}_{\perp} \end{pmatrix} d\ell \quad (1)$$

  - null space (no potl component)

Vector tomography

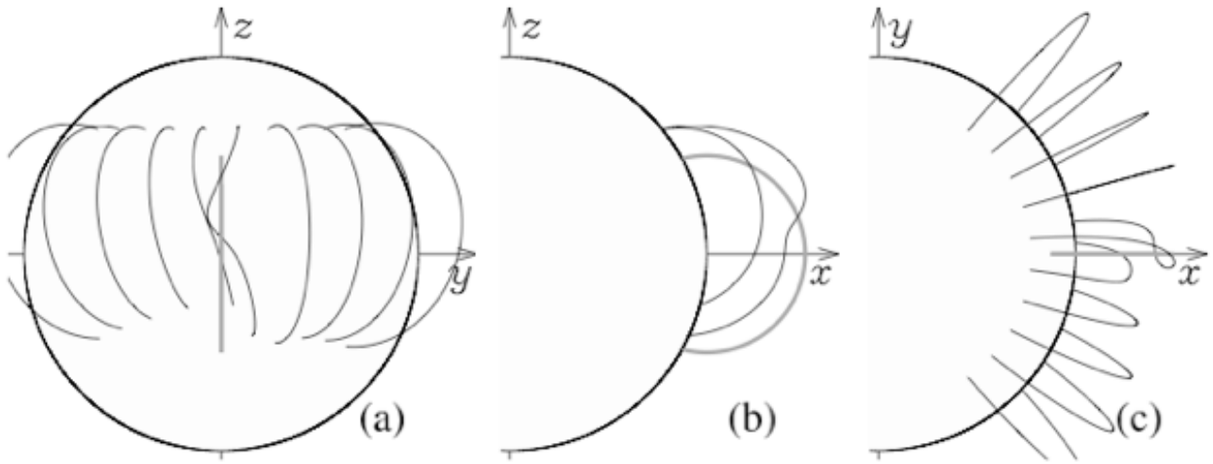

Fig. 2. Coronal magnetic field model 1 with a current loop in the meridional x, z plane. Along with the current loop we also show the distorted field lines.

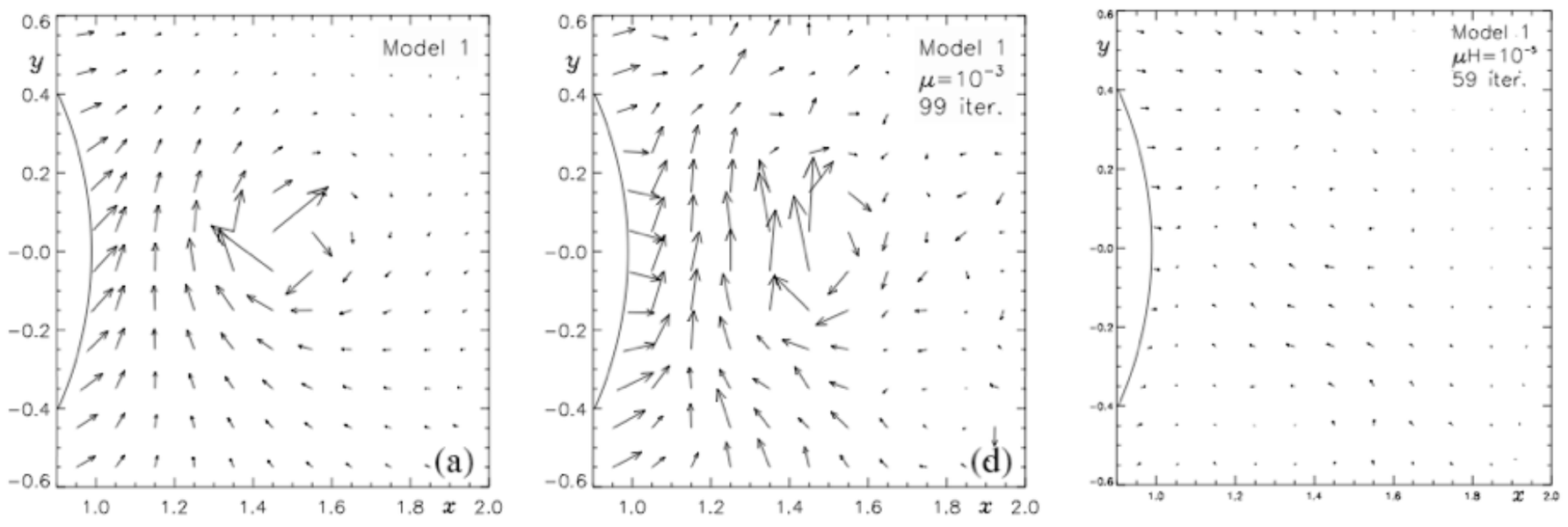

Fig. 3. Field perturbations in the equatorial plane close to where the current loop of model in Fig. 2 intersects the plane. From left to right we show the original field, the reconstruction taking only account of the Zeeman observations and of only the Hanle observations in (3).

Practical challenges and DKIST's advantages

- Measure {I + Q, I – Q} etc., sequentially in time
- Time-variable background signals ("bugs")
- Thermal background > 2 microns
- |V| << I, |Q,U| < I
- Line-of-sight
- Few photons (=> observe far from diffraction limit)
- Modest number of lines…
- Atmospheric molecular extinction, variable or steady
- Fringing amongst optical elements (instruments) – IR benefits
- (Seeing)

Fast background variations at Mauna Loa (D. Elmore)

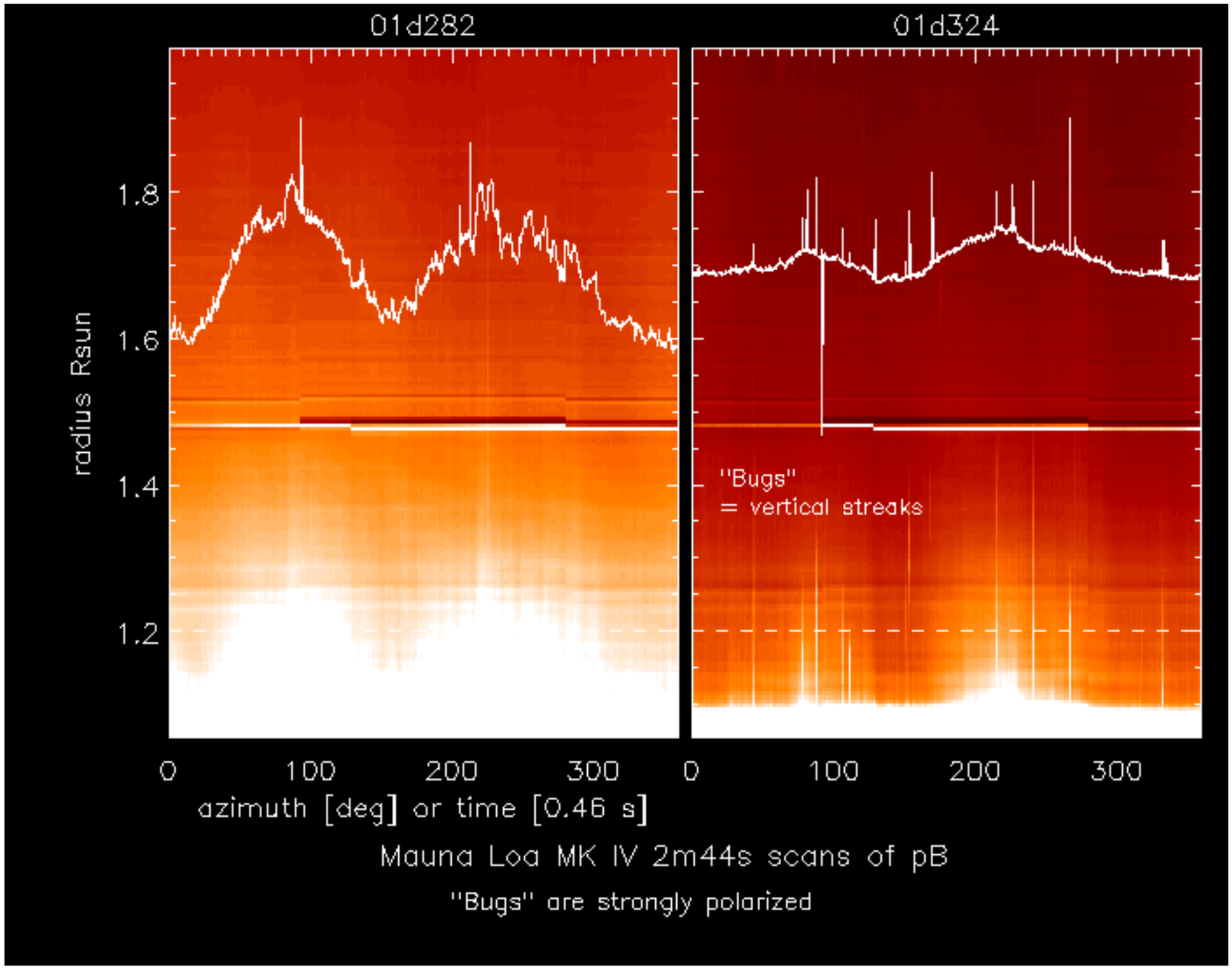

Fast background variations at Mauna Loa (D. Elmore)

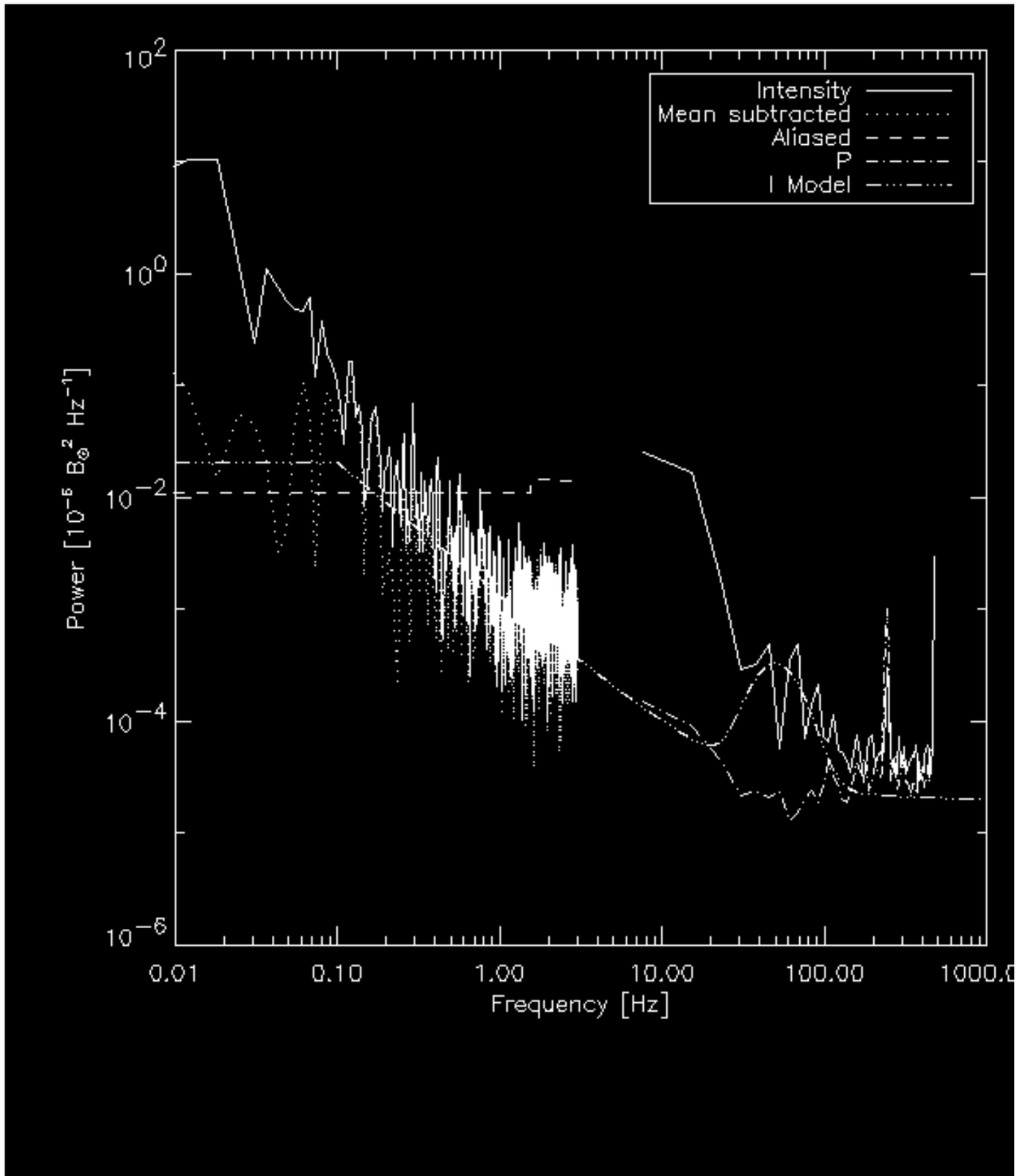

Landi Degl'Innocenti (2012 EWASS meeting):

Photospheric polarimetry is photon-starved at diffraction limit

$N_{phot} = \pi/8\ (c/\lambda^2)\ /\ (e^{hc/\lambda kT}-1)$ for Planck function B_λ at diff. limit

$= 4\ 10^6$ @ 500nm ph/sec for 10mA sampling

$N_{phot}^{-1/2} \sim 5 \times 10^{-4}$ with system efficiency 0.1

Coronal polarimetry $I_\lambda \sim 10^{-6}\ B_\lambda$

$N_{phot} \sim 10^{-6}\ \pi/8\ (c/\lambda^2)\ /\ (e^{hc/\lambda kT}-1)$

~ 4 ph/s

DKIST and Coronal Polarimetry

$N_{phot} \sim 10^{-6}\ \pi/8\ (c/\lambda^2)\ /\ (e^{hc/\lambda kT}-1)$

~ 4 ph/s

Nyqvist sampling for DKIST

μm	0.5	1	2	4	
Ny	1/80	1/40	1/20	1/10	arcsec
	9	18	36	72	km.

Target sensitivity for coronal plasmas: 10^{-4}
use px=10x diffraction limit, integrate 100 sec,
sample at 1 Angstrom, accumulate 4 10^6 photons/observation

Line of sight dB/ds . L

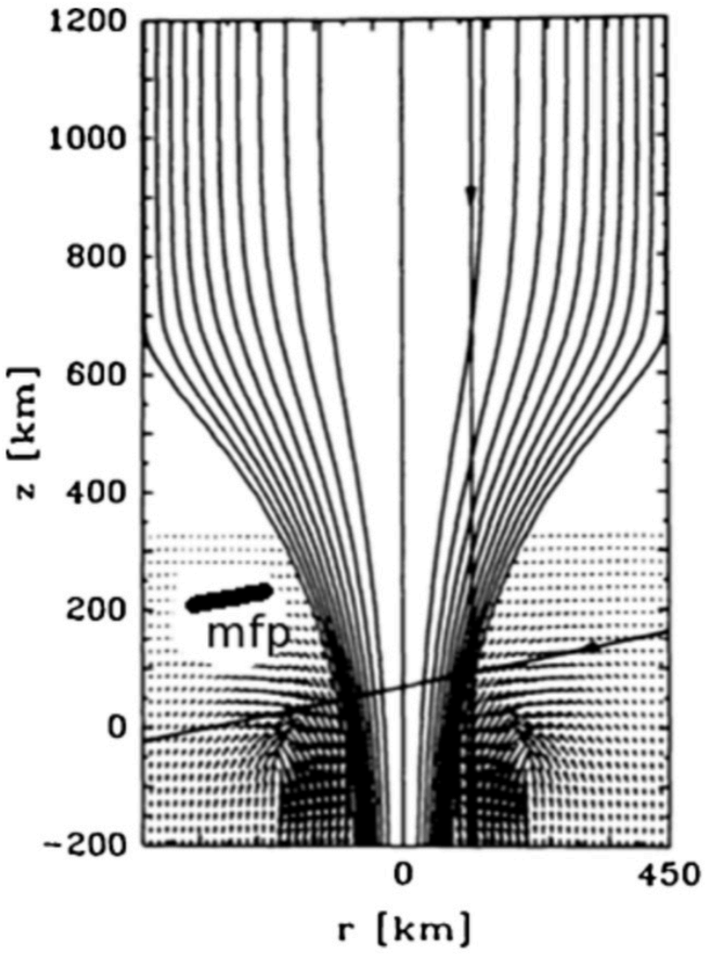

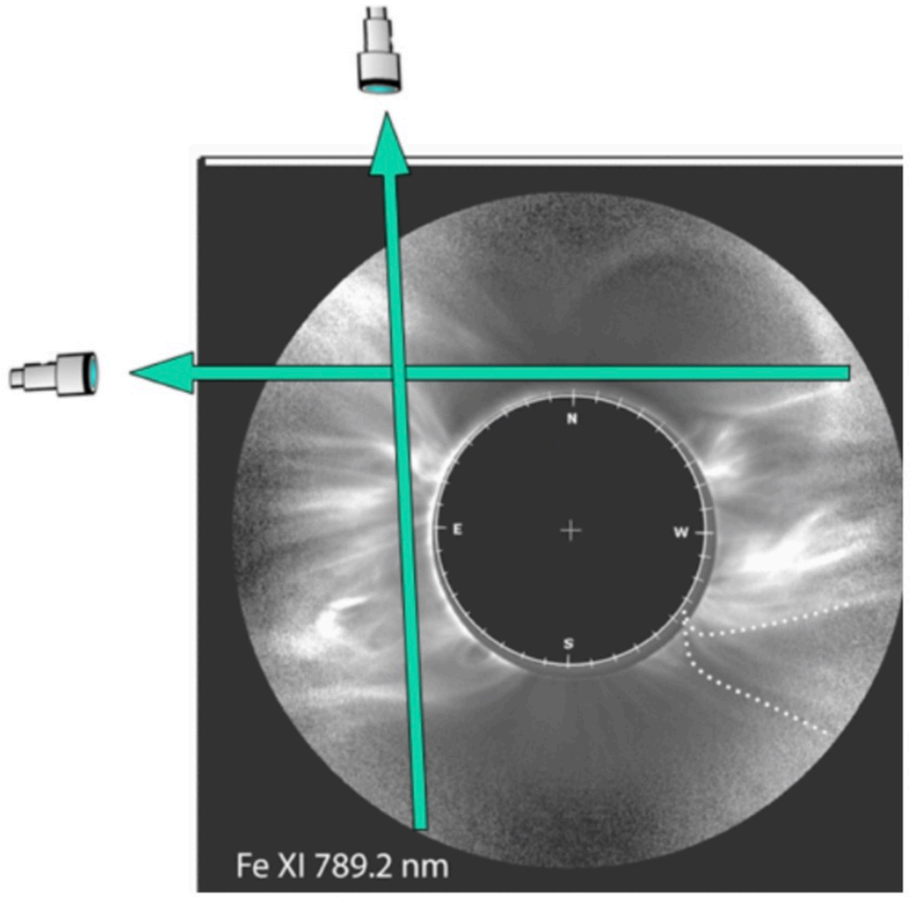

Figure 1 Left: magnetic-field lines and velocity vectors for a flux tube extending from beneath the photosphere into the chromosphere, from Steiner (1994) but annotated with the photon mean free path. Two rays intercepting the boundary between magnetised plasma are shown, along which spectral lines are formed. Right: an image of the corona during the July 2011 eclipse in the Fe XI 789.2 nm line is shown, obtained by one of us (SH). Two integration rays are shown. Note that this image already has been integrated in one dimension, thus in 3D such rays intercept much less structure than this image might seem to suggest.

Contribution functions for Cryo-NIRSP first light spectral lines

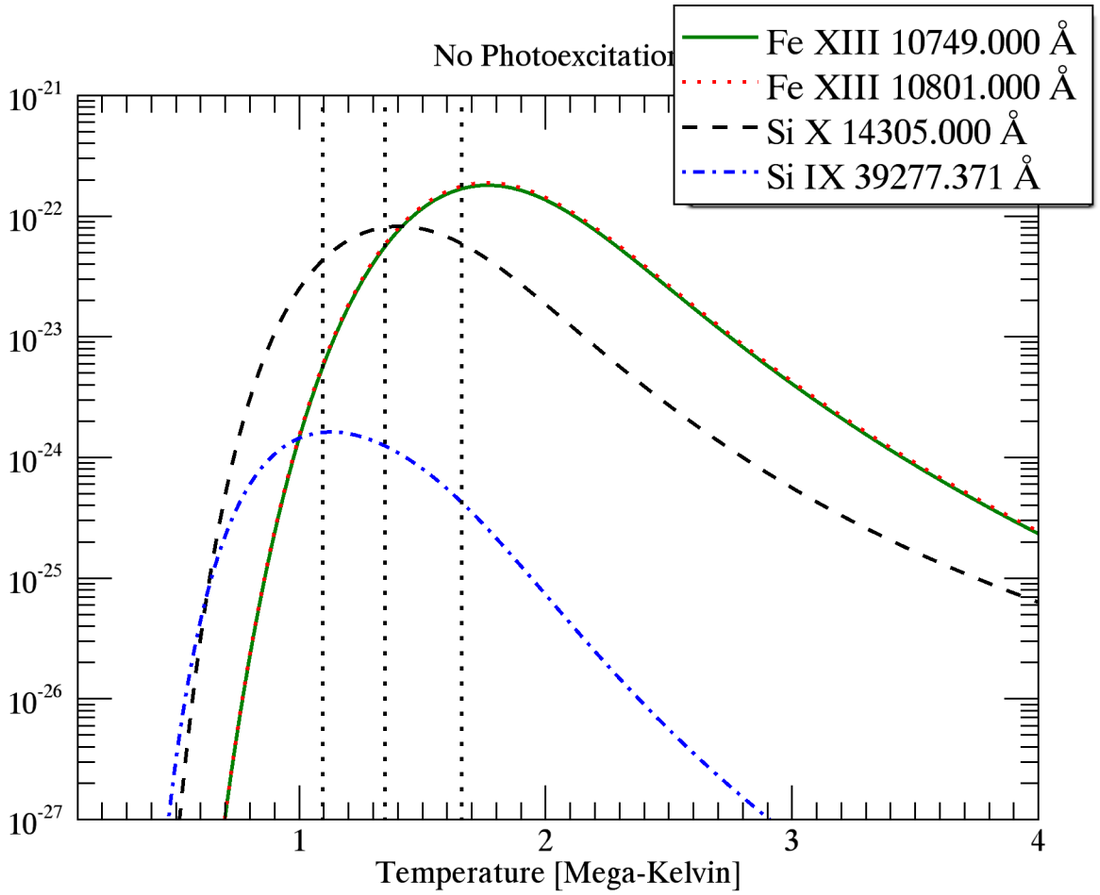

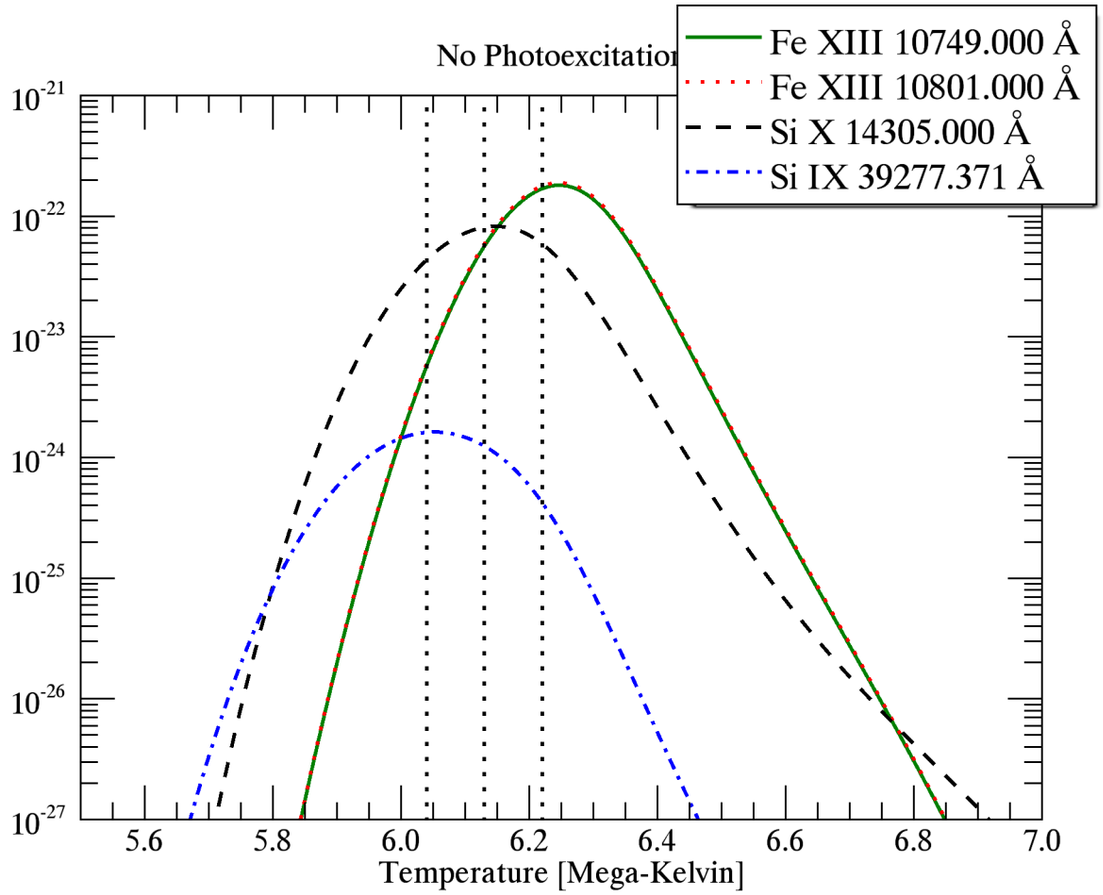

*Generated using CHIANTI v6 using default ionization equilibrium and coronal densities.

Profiles from Aircraft (47000') Air-Spec data vs Ground based (FTS) eclipse 2017

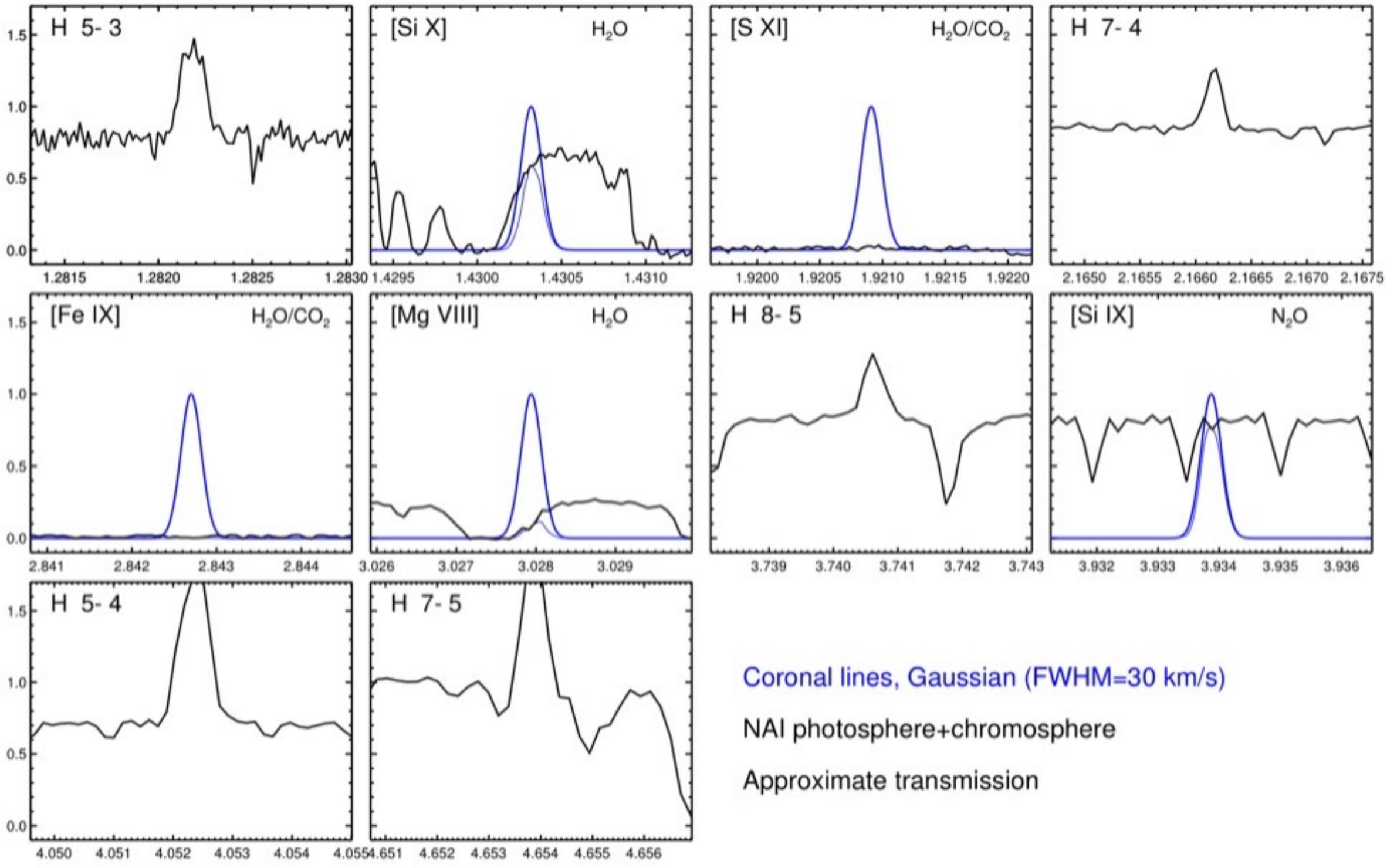

Profiles from Aircraft (47000') Air-Spec data vs Ground based (FTS) eclipse 2017

DKIST needs an FTS to scan corona/limb in IR…

- NCAR?
- Hawaii?

omnipresent fringing

Casini, Judge, Schad
2012 ApJ
Si I/ He I 1083 nm region
FIRS/DST, noise ~ 3×10^{-4}

Instrument fringe removal using 2D PCA

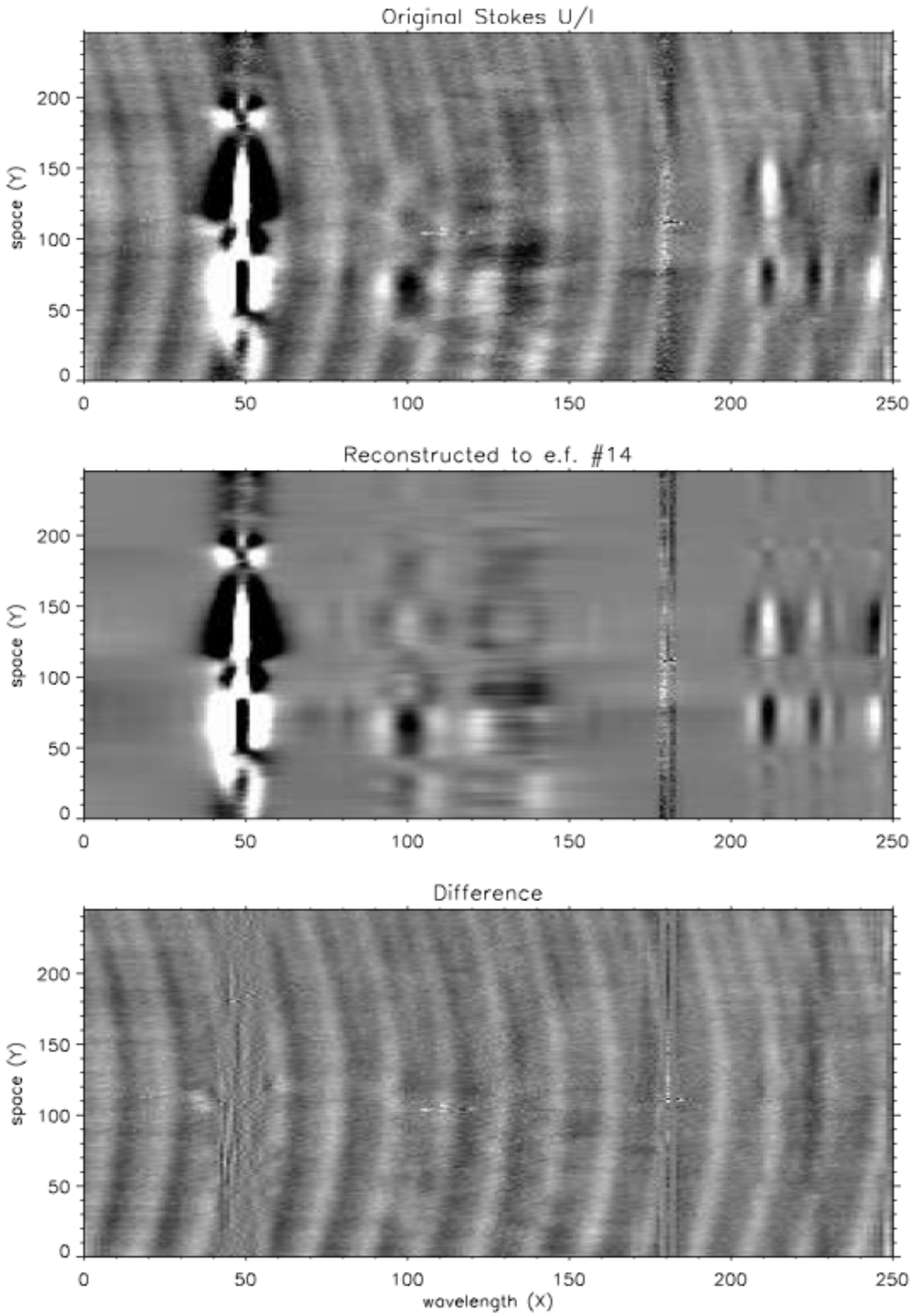

T. Schad et al He I 1083 nm as a coronal magnetic field sampler

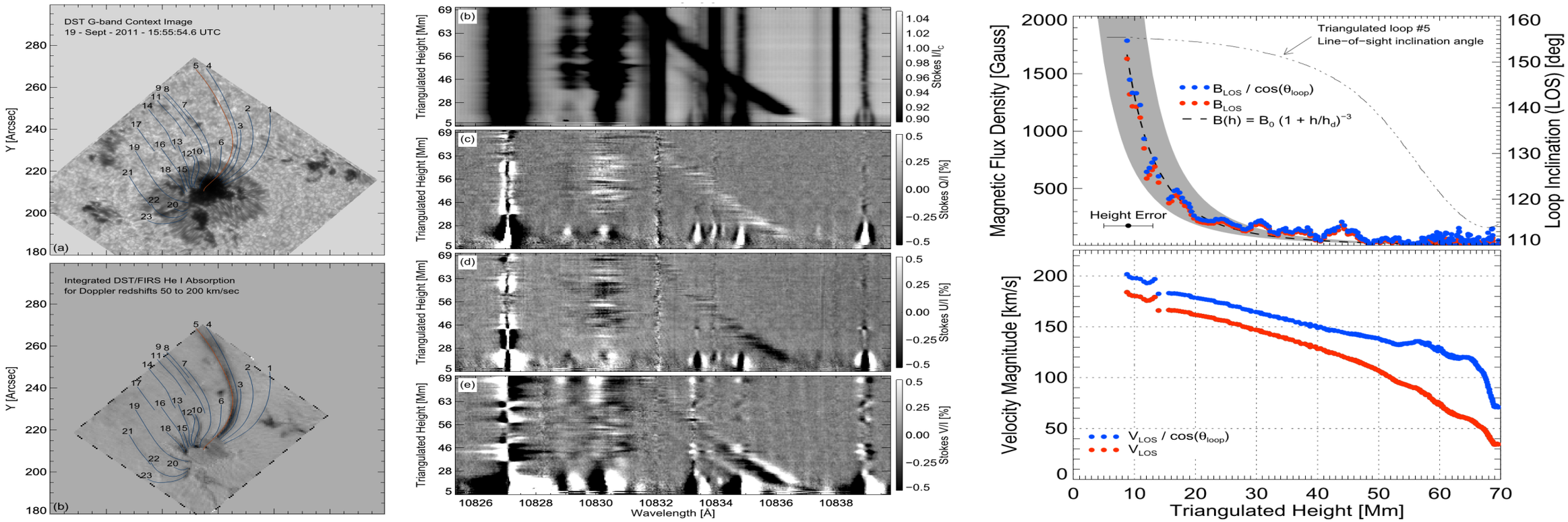

He I polarimetry of down-flowing material on disk provides vector coronal magnetic field measurements (Schad et al. 2016)

Conclusions

- **B**(x,y,z;t) is a big goal, $\partial B_i/\partial x_i$ even more so
- 3 strategies: but no silver bullet: STEREO-like s/c
- 1 point analysis: degenerate solutions to the alignment
- must add missing information
  - study various lines with vastly varying alignment (10747, 10798)
  - look for ordered minima in poln maps (Van Vleck zeros, alignment=0)
  - look for continuous vector fields in **B**(x,y,z) either from 1-point or tomographic strategies
  - regularization should remove the degeneracy for tomography
- challenging, but that is what makes it fun